Analysis of the phonon line profile of hydrogenated CdTe

2008 J. Phys.: Condens. Matter 20 325217

(http://iopscience.iop.org/0953-8984/20/32/325217)

J. Phys.: Condens. Matter **20** (2008) 325217 (9pp) doi:10.1088/0953-8984/20/32/325217

Analysis of the phonon line profile of hydrogenated CdTe

B V Robouch[1,8], P Zajdel[2,9], A Kisiel[3], A Marcelli[1], E M Sheregii[4], M Cestelli Guidi[1], M Piccinini[1,5], J Polit[4], J Cebulski[4], E Burattini[6] and A Mycielski[7]

[1] INFN-Laboratori Nazionali di Frascati, Via E Fermi 40, I-00044 Frascati, Italy
[2] Department of Chemistry, University College London, Christopher Ingold Laboratories, 20 Gordon Street, London WC1H 0AJ, UK
[3] Institute of Physics, Jagellonian University, Reymonta 4, 30-059 Krakow, Poland
[4] Institute of Physics, University of Rzeszów, Rejtana 16A, 35-310 Rzeszów, Poland
[5] Dipartimento di Scienze Geologiche, Università Roma Tre, L.go S L Murialdo, 00146 Rome, Italy
[6] Department of Informatics, University of Verona, strada le Grazie 15, I-37134 Verona, Italy
[7] Institute of Physics PAS, Aleja Lotnikow 32/46 Warszawa, Poland

E-mail: robouch@lnf.infn.it

Received 30 October 2007, in final form 9 June 2008
Published 9 July 2008
Online at stacks.iop.org/JPhysCM/20/325217

Abstract
The phonon spectrum of CdTe hydrogenated to various degrees is interpreted according to the original model, which takes into account the abundances of all naturally occurring Cd and Te stable isotopes and considers only five independent parameters to describe the 'bulk-isotope effect' line shape. The least square fitting (LSqF), unfolds the experimental data, obtained at different temperatures. The LSqF of the phonon line also considers the presence of additional oscillator contributions that we assign to vacancies or to lattice deformations occurring in the crystal.

1. Introduction

In the harmonic approximation the phonon frequency in a binary compound is inversely related to the square root of the reduced mass of a dipole ion pair, from which we get the optical phonon branch [1] dispersion formula

$$\omega_{\mathrm{opt}}^2 = \{k(M_1 - M_2) \pm [k^2(M_1 + M_2)^2 - 4k^2 M_1 M_2 \sin^2(\pi p/N)]^{1/2}\}/M_1 M_2$$

where M_1 and M_2 are the constituent masses, k is the force constant and p the phonon momentum state number ($-N/2 < p \leqslant N/2$). When phonons are excited by photon absorption, the energy typically lies in the far-infrared (FIR) region and the small momentum carried by the photons allows only transitions to states with $p \approx 0$. Thus, the above formula can be reduced to

$$\omega_{\mathrm{opt}}^2 = 2k(1/M_1 + 1/M_2). \quad (1)$$

[8] Author to whom any correspondence should be addressed.
[9] On leave from: Institute of Physics, University of Silesia, ulica Uniwersytecka 4, 40007 Katowice, Poland.

Natural crystals are a mixture of stable natural isotopes that generate an atom mass dispersion and hence different phonon frequencies. In the 1990s Cardona, using Raman spectroscopy, analysed isotope effects in the phonon spectra of Si [2], Ge [3] and ZnSe [4]. In the case of CdTe crystals, there are eight Cd and eight Te naturally stable isotopes, so a binary CdTe contains 64 different combinations of Cd–Te ion–dipole pairs, each one characterized by its reduced mass and a proper frequency. While for a ZnSe crystal grown from pure isotopes a narrow phonon line is observed [4], in crystals composed of a mixture of isotopes with various abundances, a wide and usually asymmetric phonon line is typically found. The widening occurs, as observed in CdTe, because the different isotope pairs contribute to separate components rather than acting as a single component with a frequency corresponding to that of the *average mass*.

We have shown [5] that the structure of the phonon band of CdTe depends on the amount of hydrogen collected during purification of the constituents, while during the single crystal growth process H is trapped in the CdTe lattice. In the case of CdTe with a low hydrogen content, CdTe(L), commonly

referred to in the literature as pure CdTe, the fine structure of the main phonon line of the monocrystalline CdTe is apparent. Here, we analyse the contributions from the separate isotope lines of CdTe(L).

To interpret reflectivity spectra, the Kramers–Kronig transformation is used to obtain the corresponding complex dielectric constant $\varepsilon(\omega)$ [6, 7]:

$$\varepsilon(\omega) = \varepsilon_1(\omega) + \mathrm{i}\varepsilon_2(\omega) \tag{2}$$

with

$$\varepsilon_2(\omega) = \Sigma_{j=1,n}\{S_j\, y(\omega, \omega_j, \Gamma_j)\} \tag{3}$$

where $y(\omega, \omega_j, \Gamma_j)$ is the line profile and $\{\omega_j, \Gamma_j$, and $S_j\}$ are the line frequency at line maximum, the damping constant (or the line half-width) and the (dimensionless) oscillator strength (OS) of the jth of the n spectrum components. In general for a least square fitting (LSqF), spectroscopic analysis assumes a natural Lorentzian shaped line [6]

$$^{\mathrm{L}}y_j(\omega, \omega_j, \Gamma_j) = \Gamma_j^2\omega_j\omega/[(\omega^2 - \omega_j^2)^2 + \Gamma_j^2\omega^2] \tag{4}$$

while, the response of an experimental set-up is a Gaussian shaped line [8]

$$^{\mathrm{G}}y_i(\omega, \omega_j, \Gamma_j) = \exp\{-[(\omega - \omega_j)/\Gamma_j]^2\}. \tag{5}$$

Whenever either the Lorentzian or the Gaussian line shape dominates, i.e. when $\Gamma_{\mathrm{L}} \gg \Gamma_{\mathrm{G}}$ or $\Gamma_{\mathrm{G}} \gg \Gamma_{\mathrm{L}}$, only one shape can be used. In high-resolution phonon spectroscopy analysis, an approximation by Lorentzian shape profiles is acceptable. When the two line profiles have comparable half-widths, the resulting smeared line shape is represented by a convolution of these profiles, i.e. to a good approximation by a Voigt-like shape [9]

$$^{\mathrm{V}}y(E) = \int_{-\infty}^{\infty} {}^{\mathrm{L}}y(E) *^{\mathrm{G}} y(E - E')\,\mathrm{d}E'$$

where E is the peak energy, and $^{\mathrm{L}}y(E)$, $^{\mathrm{G}}y(E)$, and $^{\mathrm{V}}y(E)$ are normalized to unity area. As this convolution integral cannot be evaluated in a closed form, numerical calculations are required. However, its application for fitting is a difficult task and for practical applications involving x-rays [10], crystallography [11, 12] and general spectroscopy [13], a linear combination of the two profiles, or a pseudo-Voigt line shape (pVoigt) is preferred

$$^{\mathrm{pV}}y(\omega, \omega_j, \Gamma_j, \boldsymbol{\eta}_j) = \boldsymbol{\eta}_j\, {}^{\mathrm{L}}y(\omega, \omega_j, \Gamma_j) + (1 - \boldsymbol{\eta}_j)\, {}^{\mathrm{G}}y(\omega, \omega_j, \Gamma_j) \tag{6}$$

with $0 \leqslant \boldsymbol{\eta} \leqslant 1$, and this formalism is more convenient for fitting procedures.

We suggest a more accurate interpretation of the FIR spectra of binary crystals, i.e. based on a mixture of all the combinations of the stable isotopes, and compare the analysis of the experimental ε_2 curves with Lorentzian, Gaussian or pseudo-Voigt profiles.

Following preliminary considerations on the CdTe spectrum [14] and an accurate investigation of both mid-IR (MIR) [15] and FIR spectra [5], we attempted a detailed analysis of the line structure.

2. CdTe isotopes

A pure *natural* CdTe crystal is composed of eight Cd and eight Te stable isotopes. The isotope of an element (El) is defined by four parameters: its atomic number, mass number (M_{El}), atomic weight and atom% abundance ($^{\mathrm{El}}p_m$). In general

$$^{\mathrm{mass\_number}}_{\mathrm{atomic\_number}}\mathrm{El}^{\mathrm{atomic\_weight}}_{\mathrm{relative\_abundance\%}}$$

and, in particular, for the eight Cd isotopes: $^{106}_{48}\mathrm{Cd}^{105.9}_{1.25\%}$, $^{108}_{48}\mathrm{Cd}^{107.9}_{0.88\%}$, $^{110}_{48}\mathrm{Cd}^{109.9}_{12.5\%}$, $^{111}_{48}\mathrm{Cd}^{110.9}_{12.8\%}$, $^{112}_{48}\mathrm{Cd}^{111.9}_{24.13\%}$, $^{113}_{48}\mathrm{Cd}^{112.9}_{12.22\%}$, $^{114}_{48}\mathrm{Cd}^{113.9}_{28.73\%}$, $^{116}_{48}\mathrm{Cd}^{115.9}_{7.49\%}$, and eight Te isotopes: $^{120}_{52}\mathrm{Te}^{119.9}_{0.1\%}$, $^{122}_{52}\mathrm{Te}^{121.9}_{2.54\%}$, $^{123}_{52}\mathrm{Te}^{122.9}_{0.9\%}$, $^{124}_{52}\mathrm{Te}^{123.9}_{4.73\%}$, $^{125}_{52}\mathrm{Te}^{124.9}_{7.1\%}$, $^{126}_{52}\mathrm{Te}^{125.9}_{18.81\%}$, $^{128}_{52}\mathrm{Te}^{127.9}_{31.73\%}$, $^{130}_{52}\mathrm{Te}^{129.9}_{34.07\%}$ [16]. The 64 possible ij-dipole ($i = M_{\mathrm{Cd}}$, $j = M_{\mathrm{Te}}$) combinations have probabilities $\{P_{ij} = {}^{\mathrm{Cd}}p_i^{\mathrm{Te}}p_j\}_{i=1,8;\,j=1,8}$. To evaluate the energy range involved, we used equation (1) to calculate the spread of the oscillator strengths, where the $\boldsymbol{\omega}(^{114}\mathrm{Cd}^{130}\mathrm{Te})$ line was fixed at 142.6 cm^{-1} (this value refers to a previous fit of [5]). We arbitrarily selected the $^{114}\mathrm{Cd}^{130}\mathrm{Te}$ isotope pair, i.e. the dominant one in terms of abundance (9.8%), as the reference 'anchor' line for resolving the remaining 63 lines. Thus the CdTe phonon frequency profile has a really fine structure with several components that, because of the limited experimental resolution, appear as a unique wide band.

As a first approximation, we assume that the elemental oscillator strengths of all the isotope mass pairs are identical and that the 64 isotope lines have.

(1) Amplitudes proportional to the product of the corresponding natural relative occurrences $\{A_{ij} = \mathbf{A}^{\mathrm{Cd}}p_i\, {}^{\mathrm{Te}}p_j\}_{i=1,8;\,j=1,8}$, with $\mathbf{A}$ the common factor of proportionality (first parameter).
(2) The same line shape with the same damping constant (or its line half-width) $\boldsymbol{\Gamma}$ (second parameter).
(3) A *proportionality factor* for each isotope pair frequency. Indeed, although the absolute values of the frequencies are unknown, the ratios of the 64 frequencies ω_{ij} are inversely proportional to the square root of the relative reduced mass ($\mu_{ij} = (1/M_i + 1/M_j)^{-1}$) of the corresponding dipoles [1], i.e. $\omega_{ij}/\omega_{i'j'} = (\mu_{i'j'}/\mu_{ij})^{1/2}$, whence $\omega_{ij} = f_0/\mu_{ij}^{1/2}$ with f_0 (third parameter).
(4) The *shift*, Δ_{shift}, anchoring the whole set of isotope lines to the dipole line of the pair $^{114}\mathrm{Cd}^{130}\mathrm{Te}$ (fourth parameter—*to put the isotope envelope into* the proper frequency position).
(5) The pVoigt mixing parameter $\boldsymbol{\eta}$, to account for the experimental dispersion ($\sim$2 cm^{-1}), which in our case is comparable to the natural line width (fifth parameter).

Hence, we will treat the whole set of isotope lines as a unique *bulk*-isotope band formed by a set of 64 similar but distinct individual contributions, well defined by masses and abundances of Cd and Te isotopes. Such an envelope is described by only five parameters (defined above), whose values are determined by the best fit of the CdTe spectrum.

The advantage of this approach is that a unique line shape—for a given compound—is used for all temperatures

and for the samples obtained with different purification techniques. It should be noted here that a previous analysis (see figure 7 in [5]) considered a set of three Lorentzians to describe the pure CdTe line shape, i.e. nine parameters for a satisfactory fit.

In a real crystal, besides the bulk-isotope contribution, point defects or impurities may also contribute to the spectrum with parasitic extra lines. To avoid overlooking any such contribution, in the best fit we tested the convergence with an overabundant set of eight *test* lines, four for each side of a spectral line. Each of the *test* lines is characterized by four independent parameters $\{A_i, \omega_i, \Gamma_i$ and $\eta_i\}_{i=1,8}$, obtained by the LSqF procedure. A returned value of $A_i = 0$ implies that the line does not exist and in the worst case only four auxiliary lines left with non-zero amplitudes occur. Lines with no amplitudes are excluded from the fit.

Depending on the quality of the fit and the consistency of the results, this approach returns more reliable estimates of additional oscillator strengths than the multiple-Lorentzian procedure, because the bulk-isotope part is always described in the same way and significantly reduces the possibility of confusing the pure CdTe contribution with defect contributions.

3. Experiment

As already reported [5, 11, 17, 18] the three samples CdTe(L), CdTe(M) and CdTe(H) here used were grown by the physical vapour transport (PVT) technique [19]. The starting polycrystalline CdTe material was grown from Cd and Te, each separately purified from oxygen contamination in a hydrogen atmosphere under pressures of 0.01, 0.1 and 0.5 atm, which we refer to as *low*(pure), *medium* and *high*, i.e. CdTe(L), CdTe(M) and CdTe(H), respectively. The samples were then heated for three days at 1023 K. Analysis of the phonon spectrum of the three samples confirmed their differences in behaviour.

The delicate purification procedure of CdTe(L) delivers homogeneous single crystals with very good electrical transport properties that fulfil the standards of detector production [19, 5, 12]. The high quality of the crystalline structure of these CdTe samples was confirmed by x-ray diffraction [15]. On the contrary, hydrogenated CdTe(M) and CdTe(H) have disordered crystalline structures [5] and exhibit poor electrical transport properties. The surfaces of all the crystals used in the experiment were polished to achieve the standards for optical experiments. Before the reflectivity experiments, the samples were heated under vacuum inside the interferometer to remove water from the surface.

The reflectivity experiments were performed at the DAΦNE-light laboratory of the Laboratori Nazionali di Frascati of the INFN [20]. We used a BRUKER Equinox 55 Fourier transform infrared (FTIR) interferometer, modified to allow spectra to be collected under vacuum ($\leqslant 10^{-3}$ mbar) with a cryogenic IRLABs bolometer. We used an Hg-lamp as the IR light source for these measurements. At the spectral resolution of 2 cm^{-1}–200 scans for a total of 15 min of acquisition time—we collected all data in the wavenumber ranges 50–600 cm^{-1} (FIR) and 550–7000 cm^{-1} (MIR) in order to have a reasonable range for the Kramers–Kronig transformation. The detailed analysis was performed in the 120–160 cm^{-1} range. We used an ARS (Advanced Research Systems Inc.) helium-cooled cryostat to cool the samples at low temperatures down to 10 K, and a liquid-nitrogen-cooled MTC (mercury cadmium telluride) detector for the reflectivity experiments in the MIR range.

We obtained the reflectivity of our samples by using as reference a gold film evaporated onto the surface of each sample. This method allows the reflectivity coefficient to be determined with an accuracy of about 1% or better. However, for almost all the samples the weak features in the vibrational spectrum observed above the background may be identified with higher accuracy [5].

4. Analysis of the phonon spectra

We analysed the CdTe FIR reflectivity spectra in the range 20–700 cm^{-1} at temperatures from 30 to 300 K. Each spectrum was carefully processed (as the experimental ω-range is finite) by using the Kramers–Kronig relation to obtain the corresponding real ε_1 and imaginary ε_2 parts of the dielectric constant ε. We first modelled the isotope effect by assuming $\boldsymbol{\omega}(^{114}Cd^{130}Te) = 142.6$ cm^{-1}, which resulted in a spread of frequencies comparable with the experimental resolution of 2 cm^{-1}. The frequency range of 130–150 cm^{-1} chosen for further analysis of the $\varepsilon_2(\omega)$ was large enough to cover the region of the expected isotope contributions. By minimizing the sum of the quadratic deviations by means of the Microsoft Office Excel 2003 Solver program, we fitted the different functions, obtaining the 'normalized sum of the quadratic deviations' or '*variance*' $s^2 = \Sigma(x_i - x_{\text{average}})^2/(n-1)$ i.e. the value determining the quality of the convergence, where n is the number of experimental entries examined.

4.1. Least square fitting of the CdTe spectra

4.1.1. Analysis of the line shape of pure CdTe at 30 K. We started with the low-temperature CdTe(L) IR reflectivity spectra in order to test the use of the pVoigt profile instead of the pure Lorentzian.

We attempted a first LSqF of the ε_2 spectrum of the CdTe(L) crystal at 30 K, ignoring the bulk-isotope shape and using only a set of eight lines (to avoid *a priori* exclusions). We assumed the lines to be successively Lorentzian, Gaussian and pVoigt (each with its variable set of parameters $\{\eta_i\}_{i=1,8}$) and with frequencies $\{\omega_i\}_{i=1,8}$ monotonically increasing within the rigid constraint of the experimental resolution: $(\omega_{i+1} - \omega_i) \geqslant 2$ cm^{-1}. This is the equivalent of the procedure used in [5], the only difference being the choice of the line shape. Data recorded at $T = 30$ K show a better contrast of the basic lines than those at room temperature (T_{room}).

The best fit returned only three lines with non-zero amplitude (pVoigt shown in figure 1(a) with its uncertainty bars). The line parameters are summarized in table 1. To illustrate the precision of the LSqF, in figure 1(a) we show the difference between the best-fit curve and the experimental data points (triangles). To avoid confusion in all subsequent figures the difference curve is omitted with only the s^2 given.

The improvement of one order of magnitude in the variance of the fit $s^2_{\text{pV}} = 1.5 (s^2_{\text{G}} = 2.1, s^2_{\text{L}} = 14.9)$ goes to supporting our procedure.

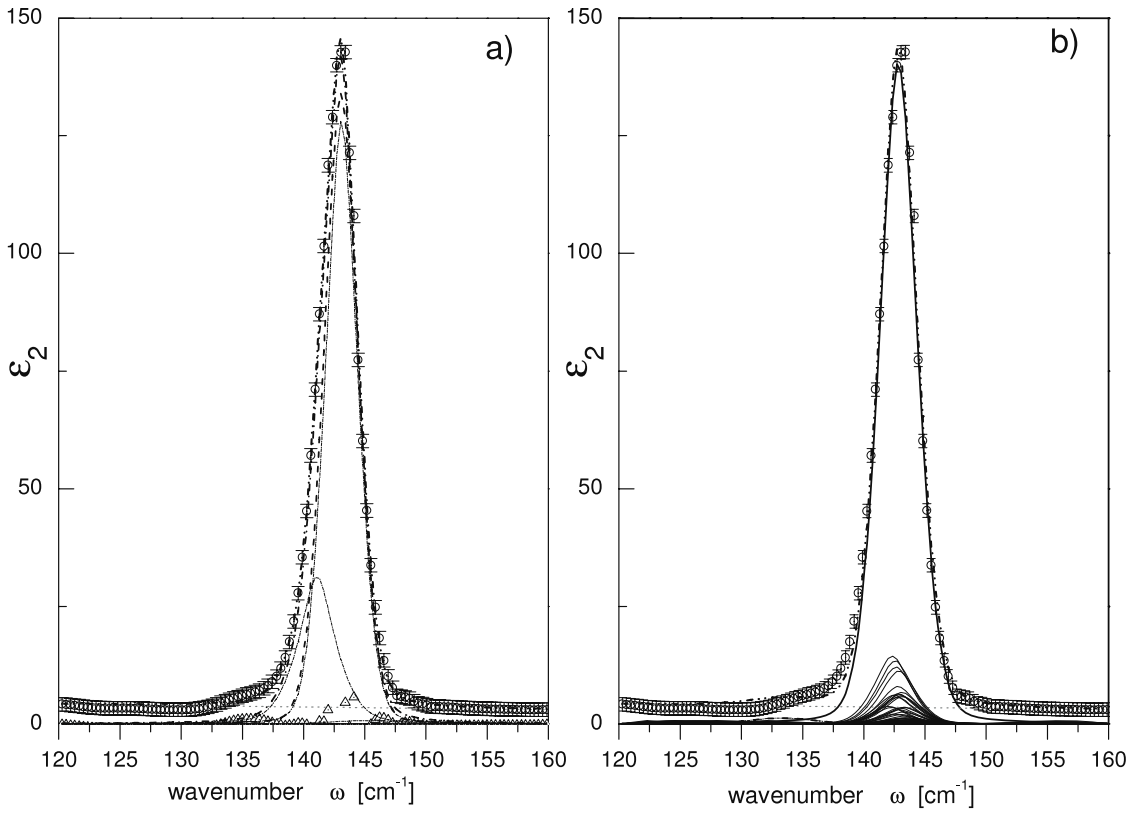

Figure 1. Kramers–Kronig transformed reflectivity spectra of CdTe(L) sample at 30 K. LSqF of $\varepsilon_2(\omega)$. In both panels: experimental data (circles with error bars); overall best fit (dash–dot–dot). (a) Best fit with three non-zero lines (solid curves), $s^2_{\rm pV} = 1.5$ ($s^2_{\rm G} = 2.1$, $s^2_{\rm L} = 14.9$) see table 1; difference between fit and experimental spectrum (solid grey). (b) Best fit with the bulk isotope and auxiliary free lines $s^2_{\rm pV} = 11.5$; (see table 2(a)): 64 individual isotope line contributions (solid); overall contribution from the 64 isotope lines (solid); overall contributions of auxiliary line (dash dot); zero line (dot).

Table 1. LSqF of the CdTe(L) ε_2 spectrum (figure 1(a)) at $T = 30$ K ($\Gamma = \langle 2; 10\rangle$ cm^{-1}) using eight pVoigt lines. $s^2_{\rm pVoigt} = 1.5$ ($s^2_{\rm Gauss} = 2.1$, $s^2_{\rm Lorenzian} = 14.9$).

ω (cm^{-1})	141.0 ± 0.2	143.1 ± 0.1	145.1 ± 0.5
A	32.8 ± 6.6	124.1 ± 4.2	2.4 ± 0.6
$\tilde{A}/\hat{A}_{\rm isotope}$	$27.5 \pm 6.9\%$	$100 \pm 0\%$	$1.8 \pm 0.4\%$
Γ (cm^{-1})	2.4 ± 0.1	2 ± 0	3.7 ± 1.0
$\boldsymbol{\eta}$	0.8 ± 0.1	0.9 ± 0.1	1 ± 0

4.1.2. Introduction to the bulk-isotope shape. We used a two-step process to carry out all further LSqFs, i.e.

- We identified the dominating contribution by fitting the 64 isotope pair envelopes, which returns the five parameters describing the bulk, while extra lines represent a higher order correction of the overall line shape.
- We performed a final fit with the auxiliary lines to identify possible non-bulk lines (figure 1(b)).

When the convergence was reached, the best fit was considered to be composed of

(a) The bulk-isotope shape = five parameters.
(b) The extra lines with non-zero amplitudes (four parameters for each line).

As already said, when auxiliary lines had no amplitude their presence was omitted. The errors were estimated by repeating the procedure in each case seven times to obtain the distribution of parameter values. This keeps to a minimum the number of parameters, and only non-vanishing lines are listed in table 2.

4.1.3. Structure of the isotope contribution at 2 cm^{-1} resolution. After obtaining the best fit of the spectrum of the crystal CdTe(L) at 30 K, we checked the structure of the bulk-isotope component obtained. Its LSqF was performed again using three different shapes and taking into account up to eight possible individual components. The best fit returned only one line with a finite amplitude and a pVoigt line shape with a preference mix $\boldsymbol{\eta} = 0.14$, i.e. an 86% Gaussian + 14% Lorentzian mixture (figure 2), while all the other contributions had no amplitudes, e.g. at our resolution the envelope was structure free. The agreement factors obtained were $s^2_{\rm Lorentzian} = 23.15$, $s^2_{\rm Gaussian} = 5.55 \times 10^{-1}$, $s^2_{\rm pV} = 8.88 \times 10^{-3}$.

Although in the general case, the isotope band contribution as obtained by fits and shown in figure 1 is slightly asymmetric, the high temperature or the effect of a limited experimental resolution may induce a broadening to appear as a single line. Under such conditions, it could well be described by a pV (pseudo-Voigt) shape with, however, a half-width and mixing parameter different from those of the individual components. In our case—as the resolution is comparable with

Table 2. LSqF of the CdTe ε_2-spectra at different T ($\Gamma = \langle 2; 10\rangle$ cm^{-1}) using first the 64 isotope pair contributions and then, in the second step, the additional eight pVoigt lines. The tables summarize the results of (a) the envelope of the bulk 64 isotope parameters and (b) the additional satellite defect lines ($\eta = 0$ G, $\eta = 1$ Lorentz).

(a)

Sample	T (K)	$A_0 \times 10^3$	Γ	η	$\omega(^{114}\mathrm{Cd}^{130}\mathrm{Te})$ (cm^{-1})	s^2_{pVoigt}	Non-zero auxiliary lines
CdTe(L)	300	1.25 ± 0.05	6.1 ± 0.1	0.09 ± 0.03	140.2 ± 0.0	0.2 ± 0.0	2
CdTe(L)	230	1.74 ± 0.03	4.1 ± 0.0	0.10 ± 0.02	141.5 ± 0.0	0.6 ± 0.0	2
CdTe(L)	100	2.76 ± 0.07	2.1 ± 0.1	0.05 ± 0.02	143.0 ± 0.0	9.6 ± 1.9	1
CdTe(L)	30	2.99 ± 0.04	2.1 ± 0.1	0.06 ± 0.01	142.9 ± 0.1	11.5 ± 0.2	1
CdTe(M)	30	4.00 ± 0.09	3.4 ± 0.1	0.05 ± 0.02	143.2 ± 0.0	7.7 ± 0.6	4
CdTe(H)	30	4.84 ± 0.14	4.3 ± 0.0	0.06 ± 0.3	142.0 ± 0.1	16.7 ± 1.0	3

(b)

Sample	T (K)		Lines observed				% of Max	# of lines
CdTe(L)	300	ω		135.7 ± 0.1		144.8 ± 0.0		
		A		1.1 ± 0.1		0.9 ± 0.1		
		$\tilde{A}/\hat{A}_{\mathrm{isotope}}$		3.7%		2.9%	3.7%	2
		Γ		2 ± 0		2 ± 0	(of 28.54)	
		η		1 ± 0		1 ± 0		
CdTe(L)	230	ω			139.9 ± 0.1	145.7 ± 0.0		
		A			0.8 ± 0.0	1.7 ± 0.1		
		$\tilde{A}/\hat{A}_{\mathrm{isotope}}$			1.4%	3.1%	3.1%	2
		Γ			2 ± 0	2 ± 0	(of 53.03)	
		η			0 ± 0	1 ± 0		
CdTe(L)	100	ω				143.8 ± 0.2		
		A				0.7 ± 0.5		
		$\tilde{A}/\hat{A}_{\mathrm{isotope}}$				0.5%	0.5%	1
		Γ				2.7 ± 0.2	(of 140.46)	
		η				0.6 ± 0.1		
CdTe(L)	30	ω			140.5 ± 0.0			
		A			6.2 ± 0.5			
		$\tilde{A}/\hat{A}_{\mathrm{isotope}}$			4.2%		4.2%	1
		Γ			2.0 ± 0.0		(of 147.57)	
		η			0.6 ± 0.1			
CdTe(M)	30	ω	131.4 ± 0.6	135.4 ± 0.5	138.8 ± 0.3	144.8 ± 0.3		
		A	1.6 ± 0.2	2.2 ± 0.2	3.8 ± 0.1	1.7 ± 0.5		
		$\tilde{A}/\hat{A}_{\mathrm{isotope}}$	1.1%	1.9%	1.8%	1.1%	1.9%	4
		Γ	2.9 ± 0.2	2.0 ± 0.0	2.3 ± 0.1	2.2 ± 0.2	(of 144.25)	
		η	1.0 ± 0.0	1.0 ± 0.0	0.9 ± 0.1	0.0 ± 0.0		
CdTe(H)	30	ω (cm^{-1})	131.8 ± 0.5	135.0 ± 0.1	137.1 ± 0.1			
		A	2.3 ± 0.5	3.3 ± 0.8	5.5 ± 0.9			
		$\tilde{A}/\hat{A}_{\mathrm{isotope}}$	1.5%	2.3%	3.7%		3.7%	3
		Γ (cm^{-1})	4.1 ± 0.6	2.5 ± 0.5	2.5 ± 0.5		(of 146.10)	
		η	0.4 ± 0.2	0.4 ± 0.2	0.4 ± 0.2			

the isotope mass dispersion—the bulk-isotope band obtained by the fit shown in figure 1(b) is well described by a single pV line. The results of the fit are illustrated in figure 2. Despite this and independently of the experimental resolution, the advantage in using the 'bulk-isotope band' is a better estimate of the half-width and mixing parameter as it accounts for a broadening which is connected with the mass dispersion. Obviously, it can be used also when the data are recorded with better resolution.

4.1.4. Temperature evolution of the CdTe (L) spectra. We applied the same LSqF procedure to the $\varepsilon_2(\omega, T)$ spectra at higher temperatures ($T = 100, 230, 300$ K), i.e. the 64 isotope pair envelope plus the eight possible pVoigt lines ($\Gamma = \langle 2; 10\rangle$) and show the results in figure 3. With increasing temperature we observe a *widening* of Γ; this behaviour, due to a shorter phonon lifetime, may be connected with the natural widening of the half-width of each component (figure 3 and table 2(a)). The fit returned only *one* non-zero auxiliary component at 30, 100 K, meaning that the successful LSqF can be performed with $5 + 4 = 9$ parameters of which five parameters are of the isotope bulk.

4.1.5. Least square fitting for highly hydrogenated samples. The spectra at 30 K of heavily hydrogenated CdTe crystals, i.e. CdTe(H) and CdTe(M), contain additional defects formed during the long growth procedure [5, 15]. The results of the analysis are summarized in figure 4 and in the last three rows of table 2(a).

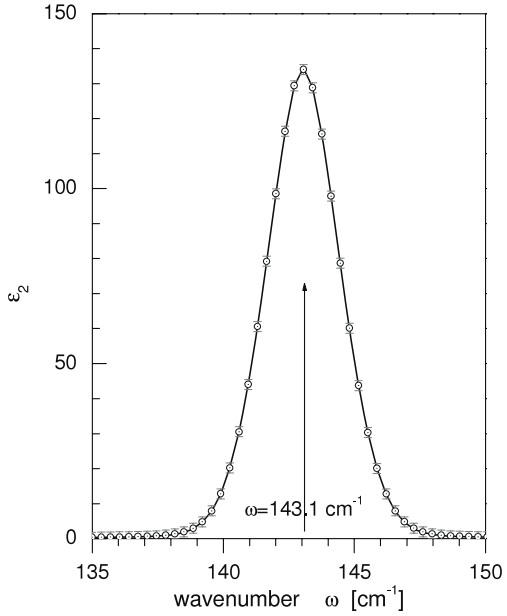

Figure 2. Single curve best-fit analysis of the bulk-isotope contribution (circles with uncertainty bars) as from the CdTe(L) sample at 30 K spectrum. pVoigt (86% Gaussian + 14% Lorentzian mix) $\omega_{max} = 143.1\ cm^{-1}$, $A_{max} = 134.5$, $\Gamma = 2.1\ cm^{-1}$, $s^2_{pV} = 8.88 \times 10^{-3}$.

5. Discussion

The choice of the line shape is critical in determining the area under the peak, e.g. the typical case of the LSqF of a phonon line split into its separate oscillator strength components. We now show the reliability of the LSqF method as based on the distribution of the component isotope pairs evaluated according to the isotope abundances and low intensity (<5%) extra lines, presumably associated with intrinsic defects. For the hydrogenated samples, we have to take into account additional *impurity*-generated lines as well as the temperature dependence of the line shape and its position. We now discuss the behaviour of the line shape, starting from that of the pure CdTe spectrum at 30 K, and its evolution versus temperature and hydrogenation.

5.1. Analysis of the line shape of pure CdTe at 30 K

The initial fits of the CdTe(L) at 30 K spectra, performed by using multiple lines without the bulk envelope, returned only three non-zero lines (table 1), whatever the line shape. The improvement of one order of magnitude in the variance of the fit $s^2_{pV} = 1.459$ ($s^2_G = 2.098$, $s^2_L = 14.934$) clearly indicates that using the pVoigt is in our case better than using the Lorentzian fit, mostly because the experimental dispersion is greater than the natural phonon line width. Although three pVoigt lines use 12 parameters, which is equivalent to four Lorentzians, but our fit returned only three non-zero Lorentzians out of eight possible values. This means that the quality of the fit cannot be improved just by adding an extra Lorentzian. In other words, the improvement to fit quality is not a function of the number of parameters but the selection of the better shape.

The LSqF of the CdTe(L) 30 K phonon spectrum returned the set of parameters of the envelope of the 64 isotope lines (figure 1(b)) of the eight test auxiliary lines only one with low intensity (<5%) was preserved by the fit. The results shown in row four of table 2(a) (isotope bulk + auxiliary lines) 142.9 ± 0.1 cm^{-1} for the dominant line in the bulk-isotope envelope $^{114}Cd^{130}Te$, agree with data shown in table 1 (multiple line fit) i.e. 143.1 ± 0.1 cm^{-1} for the strongest line of the multi-line fit.

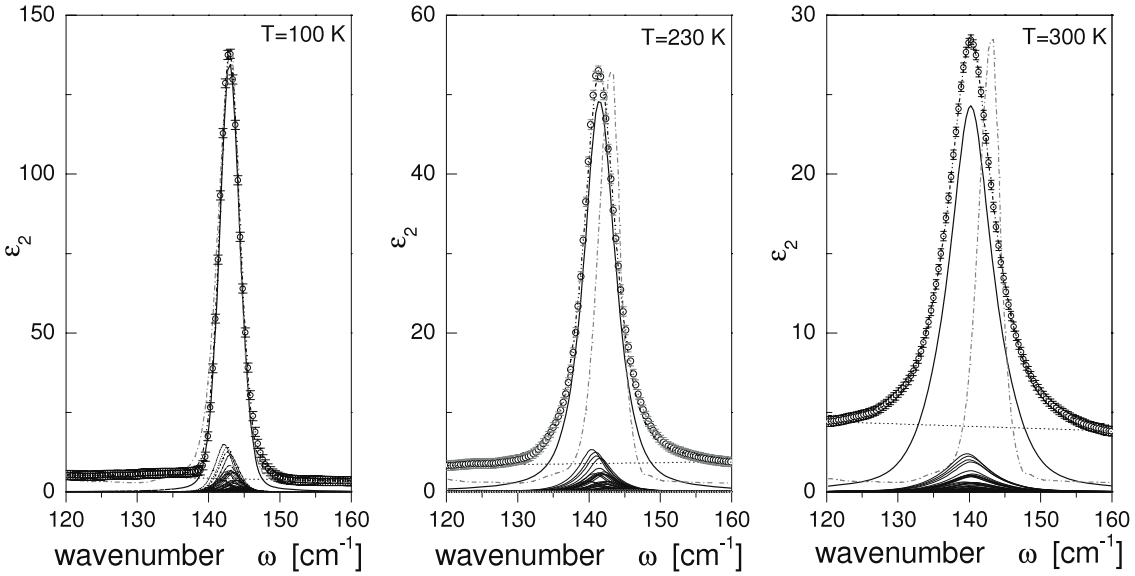

Figure 3. LSqF of CdTe(L) $\varepsilon_2(\omega, T)$-spectra assuming a 'bulk' 64 isotope line contribution plus eight pVoigt lines ($\Gamma = \langle 2; 10 \rangle$) at three different temperatures: $T = 100$, 230, 300 K. Experimental data—circles with error bars. To illustrate the thermal shift, the amplitude of the normalized 30 K curve is shown (grey dash dot). Overall best fit (dash–dot–dot); 64 individual isotope line contributions (solid); overall contribution from the 64 isotope lines (solid); individual complementary line contributions (dash dot); overall complementary line contribution (dash); zero line (dot).

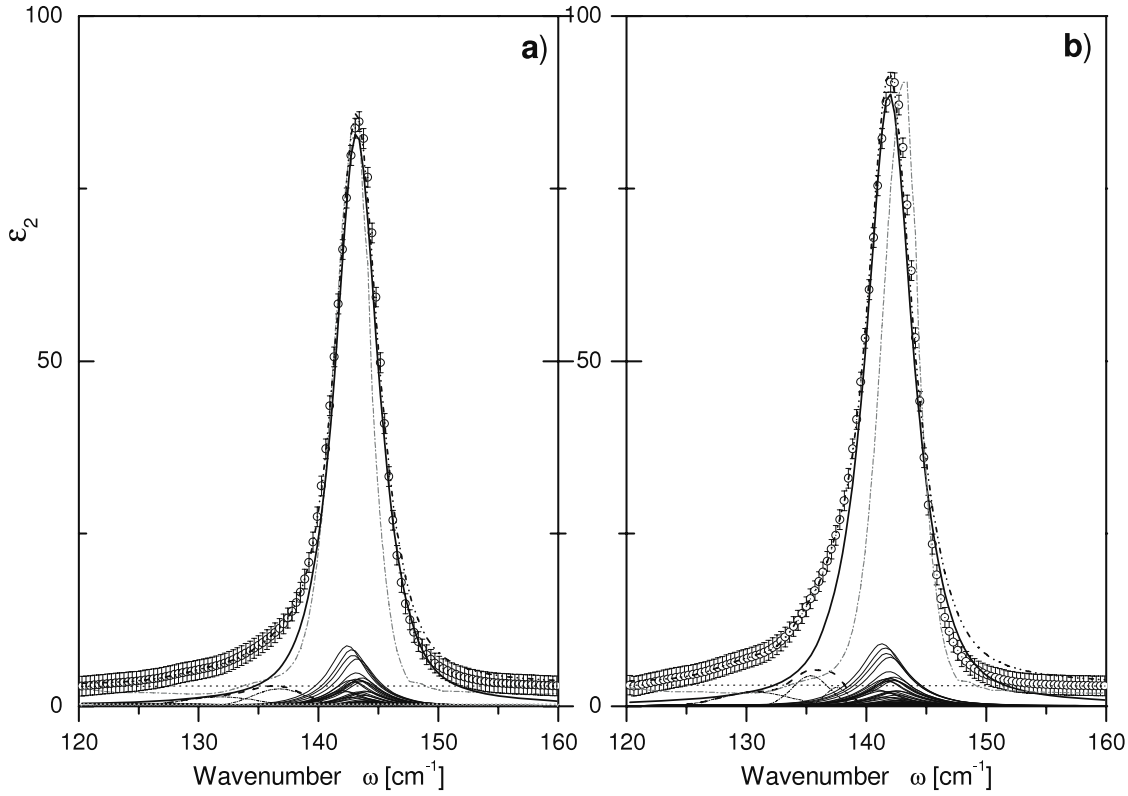

Figure 4. LSqF of the two hydrogenated CdTe samples at $T = 30$ K using 64 isotopes plus eight pVoigt lines: (a) medium ($s^2 = 7.7$), (b) heavily ($s^2 = 16.7$) hydrogenated samples. Experimental data (circles with uncertainty bars). Amplitude normalized to 30 K low-H-loaded spectrum (shown in grey dash–dot). Overall best fit (dash–dot–dot); 64 individual isotope line contributions (solid); overall contribution from the 64 isotope lines (solid); individual complementary line contributions (dash–dot); overall complementary line contribution (dash); zero line (dot).

The distribution of the 64 isotope ω_{maxima} frequency maxima covers the range $\omega_{\text{maxima}} \leqslant [142.2; 144.7]$ cm^{-1}, while the spread of distances between two successive, adjacent CdTe(L) lines $\delta\omega_{\iota,\iota+1}$ lies in the range $[0.000\,55, 0.2185]$ cm^{-1} $\ll$ 2 cm^{-1}. Actually, our experimental resolution does not allow the resolution of any fine structure. In section 4.1.3 we tried to resolve the internal structure of the fitted 'bulk-isotope envelope' by using a set of identical lines with successively Lorentzian, Gaussian and pVoigt shapes. The analysis returned only a single line with non-zero amplitude, while the additional seven *test* lines vanished (see figure 2). The quality of the procedure was monitored by the value of s^2 obtained by the fit at the convergence:

$$s^2_{\text{Lorentzian}} = 23.15 > s^2_{\text{Gaussian}} = 5.55 \times 10^{-1} > s^2_{86\%\text{Gaussian}+14\%\text{Lorentzian}} = 8.88 \times 10^{-3}.$$

again strongly in favour of the pVoigt shape. To summarize, with an experimental resolution of 2 cm^{-1} the bulk-isotope 64-line band can be described as a single line obtained with a mixture of 86% Gaussian and 14% Lorentzian ($\omega_{\text{bulk-isotope}} = 142.9 \pm 0.1$ cm^{-1}, $\Gamma_{\text{isotope}} = 2.1 \pm 0.1$ cm^{-1}) and no detectable 'fine structure' (see caption of figure 2). Again, we stress that the best fit is not the result of a greater number of available parameters (four of a pVoigt versus three of a Gaussian or a Lorentzian shape) but is due to an optimal shape. Indeed, if the fit could be improved by adding one more parameter, the procedure would return another non-zero Gaussian or Lorentzian line.

5.2. Temperature dependence of line shape for pure CdTe

At 30 K a pure CdTe(L) phonon line exhibits a quasi-Gaussian line profile ($\eta = 0$). At higher temperatures, a pVoigt shape better reproduces the experimental line. The use of the pVoigt line shape yields better fits because it accounts for both the temperature-independent experimental resolution (Gaussian) and the temperature-dependent phonon line width (Lorentzian). In our case the phonon lines show a predominantly Gaussian character ($\boldsymbol{\eta} \simeq 0$), but the Lorentzian contribution is also present. This appears evident from the result of the last four rows of table 2(a), where the parameter $\boldsymbol{\eta}$ tends to grow (in favour of the Lorentzian) with temperature $\{0.06 \pm 0.01$ at 30 K, 0.05 ± 0.02 at 100 K, 0.10 ± 0.02 at 230 K, 0.09 ± 0.03 at 300 K$\}$. On the other hand, if interpreted as a constant with a *statistical dispersion*, we would have $\boldsymbol{\eta}_{\text{average}} = 0.075 \pm 0.001 \rightarrow \langle 0.063\text{–}0.087 \rangle$. This supports the postulated increase with temperature and is in agreement with the expected increase in the damping constant Γ, which leads to the natural Lorentzian shape of vibrational lines.

The total line width remains almost constant up to 100 K and then increases by about 2 cm^{-1} every 100 K.

The initial plateau is similar to that of the forbidden band gap, which up to 100 K depends very weakly on the

temperature [21]. It is also similar to the shift of the phonon line versus temperature (see figure 8 in [15] and table 2). This correlation indicates that all of the above phenomena may be connected with each other.

At present, we are unable to explain the observed blue-shifted auxiliary lines (table 2(b)). Weak as the line amplitude is—close to the noise level—its systematic appearance probably indicates some defect in the crystal samples. The increasing number of satellite lines at higher temperatures may suggest that they are thermally activated.

The bulk-isotope contribution promptly shifts to lower energies with temperature increase (see table 2(a)). Within uncertainties, these shifts are consistent with those reported in the literature (see table 5 in [22]).

5.3. Comparison of line shapes for different purification procedures at 30 K

As already mentioned, the samples were synthesized from elements purified under different hydrogen pressures low CdTe(L) (the technological standard), medium CdTe(M) and high CdTe(H). From the fit of the bulk-isotope phonon line summarized in table 2, defects introduced by hydrogenation mainly affect the damping constant, which increases significantly from 2.1 ± 0.1 for CdTe(L) to 4.1 ± 0.0 for CdTe(M) and to 6.1 ± 0.1 for CdTe(H). The pVoigt mixing parameter remains almost constant within the fit error.

Each sample spectrum has a different number of non-zero amplitude satellite lines (table 2). The auxiliary components may have different half-widths, as they could be the convolution of an unknown number of closely stacked oscillators unresolved within the experimental resolution.

In CdTe(L) at 30 K, besides the dominant $\omega_{\text{bulk}-\text{isotope}}$ line, one satellite line with amplitude $A_{s1}/A_{\text{isotope}} \leqslant 4.2\%$ is observed in which A_{isotope} is the bulk-isotope band curve maximum (table 2(b)).

At 30 K, mainly in heavily loaded samples, static distortions are observed. The auxiliary components may have different half-widths, as they could be, within the experimental resolution, the convolution of an unknown number of closely packed unresolved oscillators. Some of the lines are found at frequencies closer to those of CdTe(L), while additional red-shifted lines appear in CdTe(M) and CdTe(H). Two effects may be responsible: thermal activation confirmed by the shift of the whole phonon band, and phonon line widening leading to a general increase in the total line width.

The attribution of extra lines to defects is evident looking at the data of the CdTe(H) sample (table 2(a), (b)), where three red-shifted lines associated with the bulk-isotope envelope were detected, but with amplitudes slightly above the noise level.

However, we want to underline that independent technological processes produced the three samples, so, the presence of internal defects and their characteristic vibration frequencies could substantially differ.

6. Conclusion

In this work we fitted the phonon spectral shape of a CdTe(L) crystal using a natural phonon line shape as determined by isotope pair abundances. The part of the oscillator strength, unaccounted for by the isotope mass dispersion, was modelled using at most four extra frequencies assigned to defects. The method returned reliable parameters for CdTe and can be generalized for any binary compound with available isotope abundances.

The advantages of our procedure, compared to the method which describes the line shape of pure CdTe using multiple Lorentzians as per [5], lie in using a well-defined 'bulk envelope' with only five free parameters, and in using a pseudo-Voigt shape of the individual component. The first improvement is to introduce an internal isotope line structure that is independent of either temperature or the purification technique. The second improvement is to account for the change in the phonon natural line width (its finite lifetime) versus the constant width of instrumental resolution. These two factors reduce the probability of assigning too much spectral weight to the *additional* lines, which could later lead to an overestimation of the number of defects.

To check the possible presence of defects in these crystals we also looked for weak extra lines. In the CdTe(L) sample, at 30 K a weak line is observed, while at higher temperatures a few extra lines appear just above the noise level.

The existence of additional lines, although with small intensity, shows that even in our *best quality* crystals some extra oscillators are present, which could be associated with point defects such as vacancies and/or anti-sites. With a resolution of 2 cm^{-1} the differences are hardly recognizable and the energies of the extra lines cannot be exactly established.

On the other hand, in samples CdTe(M) and CdTe(H), in which crystal distortions occur during growth, extra lines appear in the spectrum, with intensities higher than those in CdTe(L).

At 30 K, and below 100 K, the fit parameters $\omega(^{114}\text{Cd}^{130}\text{Te})$ (table 2) within the experimental uncertainties remain fairly constant for all hydrogen loadings, while beyond 100 K they decrease monotonically with temperature.

The fit parameter Γ has, in the case of CdTe(L), a value of about 2.1 between 30 and 100 K. The value increases with temperature (table 2(a)) as well as with hydrogen loading. Its statistical distribution returns $\Gamma_{\text{average}} = 3.2 \pm 0.6$, i.e. $\langle 2.6 \ldots 3.8 \rangle$, which indicates a widening versus loading. Such behaviour could be correlated to a shortening of the transverse optical (TO) phonon lifetime as hydrogen loading increases.

For all samples, e.g. CdTe(L), CdTe(M) and CdTe(H), the LSqF indicates that for the 64 CdTe isotope pair envelope, at low temperature the line shape is mainly Gaussian, i.e. the *instrumental* line width dominates over the *natural*. At higher temperatures, the decrease in the phonon lifetime contributes to an increase in the total width and to a consequent increase in the Lorentzian contribution to about 10%.

Acknowledgment

Part of this work was supported by the EU TARI-project contract HPRI-CT-1999-00088.

References

[1] Wannier G H 1959 *Elements of Solid State Theory* (Cambridge: Cambridge University Press)
[2] Wang D T, Gobel A, Zegenhagen J and Cardona M 1997 *Phys. Rev.* B **56** 13167
[3] Gobel A, Wang D T, Cardona M, Pintschovius L, Reichard W, Kudla J, Pyka N M, Iton K and Haller E E 1998 *Phys. Rev.* B **58** 10510
[4] Gobel A, Ruf T, Zhang J M, Lauck R and Cardona M 1999 *Phys. Rev.* B **59** 2749
[5] Polit J, Sheregii E M, Robouch B V, Marcelli A, Cebulski J, Cestelli Guidi M, Piccinini M, Kisiel A, Zajdel P, Burattini E and Mycielski A 2006 *J. Appl. Phys.* **100** 13521
[6] Stern F 1968 *Solid State Phys.* **15** 299
Flugge S (ed) 1970 *Encyclopaedia of Physics* (Berlin: Springer) p 190 XXV/2c Light and matter 1 Eq.VII.4.19
[7] Taylor D W 1988 *Optical Properties of Mixed Crystals* ed R J Elliot and I P Ipatova (Amsterdam: Elsevier) pp 35–131
[8] Parratt L G 1959 *Rev. Mod. Phys.* **31** 616
[9] Voigt W 1912 *Sitz. Berg. Math. Nat. Kl. Bayer. Akad. Wiss. Munchen* **42** 603–20
[10] Werheim G K, Butler M A, West K W and Buchanan D N E 1974 *Rev. Sci. Instrum.* **45** 1369
[11] Thompson P, Cox D E and Hastings J B 1987 *J. Appl. Crystallogr.* **20** 79
[12] Sánchez-Bajo F and Cumbrera F L 1997 The use of the pseudo-Voigt function in the variance method of x-ray line-broadening analysis *J. Appl. Crystallogr.* **30** 427 http://dx.doi.org/10.1107/S0021889896015464
[13] Vegh J 2005 *Rev. Sci. Instrum.* **76** 056107
[14] Kisiel A, Robouch B V, Burattini E, Marcelli A, Piccinini M, Cestelli Guidi M, Calvani P, Nucara A, Sheregii E M, Polit J and Cebulski J 2003 *5th Int. Ural Seminar Radiation Damage Physics of Metals and Alloys (Snezhinsk)* (Book of abstracts)
[15] Zajdel P, Kisiel A, Polit J, Robouch B V, Sheregii E M, Warczewski J, Cebulski J, Burattini E, Marcelli A, Cestelli Guidi M, Piccinini M and Mycielski A 2006 *J. Alloys Compounds* **426** 12–21
[16] Rosman K J R and Taylor P D P 1998 *Pure Appl. Chem.* **70** 217
[17] Polit J, Kisiel A, Mycielski A, Sheregii E, Cebulski J, Piccinini M, Robouch B V, Marcelli A, Cestelli Guidi M and Nucara A 2005 *Phys. Status Solidi* c **2** 1147
[18] Polit J, Sheregii E, Cebulski J, Kisiel A, Piccinini M, Robouch B V, Cestelli-Guidi M, Nucara A and Mycielski A 2006 *Infrared Phys. Technol.* **49** 23
[19] Mycielski A, Szadkowski A, Łusakowski E, Kowalczyk L, Domagała J, Bąk-Misiuk J and Wiliamowski Z 1999 *J. Cryst. Growth* **197** 423
[20] Cestelli Guidi M, Piccinini M, Marcelli A, Nucara A, Calvani P and Burattini E 2005 *J. Opt. Soc. Am.* **22** 2810
[21] Hrostowski H J 1959 *Semiconductors* ed N B Hanney (New York: Reinhold) pp 437–81
[22] Danielewicz E J and Coleman P D 1974 *Appl. Opt.* **13** 1166